Anomalous Diffusion of High Molecular Weight Polyisopropylacrylamide in Nanopores

Yaron Caspi,[†] David Zbaida,[†] Hagai Cohen,[‡] and Michael Elbaum*,[†]

Department of Materials and Interfaces and Department of Chemical Research Support, The Weizmann Institute of Science, Rehovot 76100, Israel

Received June 4, 2008; Revised Manuscript Received November 12, 2008

ABSTRACT: Passage of polymers through pores narrower than the hydrodynamic diameter is impeded by an entropic penalty for their confinement. This might be balanced by an attractive interaction with the pore walls. We found that the hydrogen-bonding polymer, poly(isopropylacrylamide) (pNIPAM), diffused readily through narrow pores in polycarbonate track-etched membranes. The *trans* side accumulation of pNIPAM followed a stretched exponential behavior. By contrast, a much smaller dextran diffused at a comparable or slower rate and showed ordinary Fick-like behavior. Comparison between the influence of pNIPAM surface adsorption and chemical grafting to the pores points to weak interpolymeric bonds as the source for the transport-accelerating surface interactions. We interpret the results as evidence for anomalous diffusion of pNIPAM inside the pores.

1. Introduction

Polymers in confined geometries play an important role in many natural occurring phenomena and technological applications, ranging from viral DNA packaging and biological transporters of proteins and sugars to size exclusion chromatography. The fundamental importance of the subject has stimulated extensive research regarding both static and dynamic properties of confined polymers.[1] Cylindrical pores are particularly convenient for theoretical and experimental studies. As long as the pore is much larger than the polymer, the latter can be modeled approximately as a hard sphere with an effective hydrodynamic radius. In that case, the intrachannel diffusion can be described by the simple relation $D_p = HD_\infty$, where D_∞ and D_p are the diffusion constants in the bulk and inside the channel, respectively. The hindrance diffusion factor (H) is the product of the partition coefficient Θ to reside in the pore and the intrapore hindrance diffusion factor (H_D) that describes the influence on the solute diffusion due to hydrodynamic and chemical interactions, i.e., $H = \Theta H_D$. The exact dependence of H_D on the solute to pore size ratio has been the subject of detailed experimental[2−5] and theoretical work[6,7] over the past decades. Obviously, in the hard wall case both Θ and H_D go to zero as the solute scale approaches the pore diameter.

Beyond the hard sphere approximation, polymers may deform in order to enter confined volumes smaller than their bulk size.[8,9] However, such confinement involves an entropic penalty that is manifested in the relation $F = -k_BT \ln(\Theta)$, where F is the free energy of the polymer, k_B the Boltzmann constant, and T the temperature. Scaling theory and detailed calculation predict that $F \sim k_BT(\Lambda)^{5/3}$ and $H_D \sim \Lambda^{-2/3}$, where Λ is the ratio between the polymer gyration radius and pore radius.[10,11] Thus, if a polymer is much larger than the pore, the fraction of chains that will pass through the pore is negligible.

Polymers can be forced to enter narrow pores if driven by some thermodynamic force, such as osmotic pressure.[12,13] In these cases, the passage times may be faster than in bulk solution.[14] Another means to change the functional dependence of both H_D and Θ on Λ is to introduce an external energy term to F, e.g., attractive interactions between the polymer and the pore walls.[15] For short-range interactions, a phase transition occurs as the interaction energy is increased,[16] and a critical adsorption regime is reached when the enthalpic gain becomes comparable to the entropic penalty. In this regime Θ shows only a moderate dependence on Λ, and the polymer is partially extended along the walls. At the critical point of adsorption the surface energy exactly balances the entropic penalty. For a Gaussian chain, Θ_{cr} is independent of Λ, while for a self-avoiding random walk polymer a moderate Λ dependence is predicted even at the critical point.[17,18] Upon further increase of the surface energy, the adsorption regime is reached, Θ grows exponentially with Λ, and chains prefer to reside inside the pores.

Polymer residence in narrow pores due to surface interactions was previously observed experimentally.[19] In fact, the phenomenon is routinely exploited in adsorption liquid chromatography, where critical adsorption conditions are applied in order to separate molecules according to some chemical quantity distinct from their molecular mass distribution.[20]

Similar thermodynamic considerations that predict a phase transition were applied to consider the state of polymers next to adsorbing flat surfaces.[21] Recently, fluorescence correlation spectroscopy[22] and atomic force microscopy[23] were used in order to probe the dynamics of surface-adsorbed polymers. These measurements suggested a reptation movement along the surface (a snakelike diffusion of the polymer along its contour). The diffusion constant was shown to depend on the number of Kuhn length segments in the chain as $N^{-3/2}$.[22] Computer simulations confirm this behavior and predict that the polymer should remain mobile even if the adsorption energy is twice the critical value.[24] Yet, while some simulations emphasized the importance of reptation as the leading diffusion mechanism on adsorbing surfaces,[25] others have claimed that it probably does not play an important role.[26,27] Simulations also confirm the power-law dependence of the diffusion constant on adsorption strength and predict in addition a dependence on surface corrugation.

Multiple interactions in polymer adsorption suggest an additive or synergistic effect on adsorption. Thus, the total interaction may be strong even if individual bonds are weaker than k_BT, and adsorption of long polymers should be effectively irreversible. Indeed, surface-adsorbed polymers do not spontaneously solubilize even into good solvent. When exposed to a polymer solution, however, a piecewise exchange can occur when binding of one chain is displaced locally by binding of

* Corresponding author: e-mail michael.elbaum@weizmann.ac.il.
[†] Department of Materials and Interfaces.
[‡] Department of Chemical Research Support.

10.1021/ma801248a CCC: $40.75
Published on Web 01/08/2009

another at the former attachment site. This can lead to desorption that would not have occurred into the polymer-free solvent.[28,29] The adsorption−desorption exchange process may remain out of equilibrium for long durations, which further lowers the apparent energy gap between adsorbed and desorbed states.[30] Thus, the local environment plays an essential role in determining exchange and desorption kinetics.

In contrast to the active interest in the dynamical properties of macromolecules on adsorbing substrates, and the large body of work on the partitioning of macromolecules into adsorbing pores, the effect of surface interactions on diffusion in confined geometries has received less attention. Two computer simulations observed that the chain mobility is not suppressed even for the strong adsorption case and that the intrapore diffusion constant remains of the same order of magnitude as the bulk value.[31,32] In addition, surface interactions in confined pores decreased the glass transition temperature of a polymer solution and accelerate, by up to 2 orders of magnitude, the segmental relaxation dynamics, as long as the pore size was not too small (∼3 nm).[33]

In an interesting application to biological transporters, it was proposed theoretically that different scaling of the adsorbing fraction and the diffusion rate with interaction strength leads to an optimum in transport flux.[34] This phenomenon was also suggested to explain the selectivity of the eukaryotic nuclear pore for large protein complexes in exchange between the cell nucleus and cytoplasm, which is thought to depend on weak interactions between transport proteins and natively unfolded polypeptides.[35−39] This biological system served as an important conceptual inspiration for the present study.[40]

In the above theoretical and experimental works an intrapore ordinary diffusion process was observed, consistent with Fick's law that flux is simply proportional to the gradient in concentration. However, deviations from ordinary diffusion might be expected if the diffusing agent is subject to multiple trapping along its transit path, e.g., due to short-ranged attractive interactions. In such cases, the molecular diffusion may be anomalous, where the mean-square displacement is proportional to t^{α} and $\alpha \neq 1$.

In order to address the issue of intrapore diffusion with polymeric solute−surface interactions, we explored the behavior of polyisopropylacrylamide (pNIPAM) in passage through narrow pores. pNIPAM is well-known for its intramolecular hydrogen bonding and its hydrophilic−hydrophobic phase transition at 32 °C. At elevated temperature the condensed phase appears, while below the transition temperature the polymer is soluble. The phase transition is induced by an interplay between the entropy of the polymer and the surrounding water molecules and the enthalpy that results from hydrogen bonding of amide moieties and hydrophobic interactions among the isopropyl groups.[41] In fact, even below the transition hydrogen bonds may form between the monomers[42] or with other solutes.[43] As result, the collapse process of the homopolymer is composed of a series of substages with an increasing number of internal monomer−monomer interactions and a gradual decrease in overall size.[44] This picture is consistent with a coexistence of free and hydrogen-bonded monomers below the transition and is also manifested in the dynamics of the collapse process. For example, two distinct time scales were observed when their collapse was induced by methanol[45] or by an infrared laser:[46] a fast one that corresponds to crumpling of the chain and a slow one associated with conversion of the crumpled chain to a compact globule.

Interestingly, the adsorption of pNIPAM on poly(*N*-*tert*-butylacrylamide) latex particles in water was found to take place through occasional hydrogen bonds; the polymer was left in a loopy conformation with sparse polymer−particle contacts relative to the number of monomers.[47,48] When the adsorbed polymer was heated to 60 °C and cooled again, a reversible transition from globule to extended to loopy phases was observed with sluggish, stretched exponential dynamics. On the basis of these previous works, we reasoned that pNIPAM may provide the requisite weak interaction while retaining high mobility in solution.

In this work, diffusion of pNIPAM through narrow pores was tested in a simple transport experiment. A commercial polycarbonate track-etched filter separated between two liquid-filled chambers. Polymer was introduced on the *cis* side, and its accumulation on the *trans* side was detected by fluorescence in real time. The membrane thickness was much larger than the polymer hydrodynamic diameter. We compared the diffusion kinetics when the polymer was much smaller than the pore size (50 nm diameter) to cases where it was comparable (200 nm) or larger (1000 nm). We found that pNIPAM passes through pores much smaller than its hydrodynamic diameter, that the rate of passage is faster than that of a much smaller dextran, and that accumulation on the *trans* side of narrow pores follows anomalous kinetics.

2. Experimental Section

Materials. Hydrazine was purchased from Merck. Organic solvents were purchased from Bio-Lab (Israel) or Merck. Polyvinylpyrrolidone (PVP)-coated polycarbonate membranes were purchased from SPI Supplies. All other materials were obtained from Sigma Aldrich. Isopropylacrylamide was dissolved in toluene and precipitated from hexane before use. All other compounds were used without further purification.

Synthesis of Methacryloxysuccinimidyl Ester (MASI). Methacrylic acid (5 g), *N,N′*-dicyclohexylcarbodiimide (DCC) (12 g), and *N*-hydroxysuccinimide (6.8 g) were dissolved in tetrahydrofuran (THF) (170 mL) and stirred overnight. The solution was filtered off, and the solvent was evaporated. The received solid was recrystallized from boiling *n*-heptane to obtain MASI, melting point 101 °C.[49]

Synthesis of Fluorescent Tag Grafted Polymer. Co-pNIPAM polymers were polymerized by free radical polymerization in dimethylformamide (DMF) using 1,1′-azobis(cyclohexanecarbonitrile) (ACBN) as an initiator. For polymer 1 we used monomers of isopropyacrylamide, methacryloxysuccinimidyl ester, and [3-(methacryloylamino)propyl]triethylammonium chloride in a molar ratio of 97:1.5:1.5. Reagents were added to argon-degassed *N,N*-dimethylformamide (DMF) (40 mL) (total concentration 1.77 mM). The polymerization was carried out overnight at 85 °C. The DMF was evaporated, and the crude product was recrystallized from THF:diethyl ether.

Polymer 1 (126.3 mg, 5.3 μmol) was reacted at room temperature with hydrazine (134 μg, 2.7 mmol) in ethanol (5 mL) overnight. The hydrazine:MASI monomers molar ratio was 30:1. The obtained hydrazide derivative polymer 1 was recrystallized in THF:diethyl ether.

The hydrazide polymer derivative (100 mg in 5 mL, 0.1 M sodium bicarbonate, pH 8.5) was reacted with fluorescein isothiocyanate (FITC) (7.43 mg) dissolved in DMSO (800 μL) overnight in darkness, using FITC:hydrazide monomers in molar ratio of 1.5:1. The solvent was evaporated, and the crude product was resuspended in water. It was then purified on a G-25 size exclusion chromatography column (Amersham Pharmacia). Polymer 2 was polymerized according to a similar procedure with isopropyacrylamide, methacryloxysuccinimidyl ester, and the cross-linker *N,N′*-methylenebis(acrylamide) in a molar ratio of 97.5:1.5:1.

Characterization of Fluorescent Tagged Polymers. (a) Light scattering was recorded using a custom-built setup in the Chemical Research Support Department of the Weizmann Institute (Spectra Physics 164-05, Lexel Laser 5164AR-FS tube, 7 W; ITT FW130 photomultiplier; Brookhaven BI-2030AT correlator). Data were analyzed using the CONTIN algorithm. (b) Specific viscosity was measured using a rotating plate viscosimeter (Roto Visco 1 -

Table 1. Membranes Used in This Study: Manufacturer's Specifications

pore size (nm)	SPI catalog number	density of pores (pores/cm^2)	thickness (μm)
50	E0053-MB	6×10^8	6
200	E0213-MB	3×10^8	10
1000	E1013-MB	2×10^7	11

Thermo Haake). Temperature was kept at 20 °C using water flow from a thermal bath. Viscosity was measured at shear rates of 810−1260 s^{-1} in steps of 14 s^{-1}.

Characterization of the Polycarbonate Membranes. Polycarbonate track etch membranes used in this work are listed in Table 1.

For adsorption assays, membranes were incubated in 10 mM sodium phosphate buffer pH 7.5 in the presence of 25−270 μg/mL of the relevant polymers for at least 1 day and were washed twice for 1 day in the same buffer. Membrane images were recorded using the blue channel of an Olympus Fluoview 300 confocal microscope with UPlanSApo 60× objective (Olympus Europe, Inc.). The depth scan colocalization image was constructed using the colocalization plugin of ImageJ[50] by inverting the intensity of the transmission figure, forming a colocalized figure, and merging the transmission (in red), fluorescence (in green), and colocalization (in white) channels into RGB space. Points were considered colocalized if their intensities were strictly higher than the threshold of their channels (50 out of 255 in an 8-bit picture) and their intensity ratio was strictly higher than 70%.

Pore sizes were measured using a custom-built water flow apparatus. A membrane was sealed as a lid on a one-sided chamber, which was then evacuated. A measured volume of water (0.5 or 1.0 mL) was added above the membrane at atmospheric pressure, and the flow time was recorded. Temperature was held constant by a water jacket attached to a circulating thermostat (Lauda RE104). The effective pore size was found using the known exposed area of the membrane, the pore density, and Poiseuille's law $J = (nR_p^4/8\eta L)\Delta P$. Here, R_p is the pore radius, L the width of the membrane, n the number of pores, η the solvent viscosity, and ΔP the trans-membrane pressure gradient.

Grafting pNIPAM on Polycarbonate Membranes. Milli-Q water was degassed with argon for at least 3 h to exchange dissolved oxygen, and NIPAM monomers were dissolved to a final concentration of 5% under argon atmosphere. Glass flasks were flushed with argon, filled immediately with 5 mL of the NIPAM solution, and sealed. Four or five membranes were placed on a Petri dish inside a MARCH plasmod plasma generator equipped with a GMS 200 controller and an EMI RF generator. The plasma chamber was pumped to ∼400 mTorr, and argon was flushed inside at a rate of 0.5 cm^3/min. Plasma treatment was operated for 4 min at 50 W. Membranes were transferred to the NIPAM solution (one membrane per flask), and the polymerization was carried out for 12 h at 29 °C on a belly shaker. Finally, the membranes were washed twice in Milli-Q water for 16−24 h and dried in an oven for 6 h at 40 °C.

Membrane Transport Experiments. Membrane transport experiments were performed on a custom-built fluorescence microscope, using a water dipping objective for fluorescence collection (Olympus LUMPLFL 100XW), a blue light emitting diode (LED) as the excitation source (RL5-B5515, Superbright leds), filters for FITC fluorescence (SEMROCK FITC-3540B filter set), and a photomultiplier (Hamamatsu, H6180-1) for detection (see Figure S1a of the Supporting Information). A National Instruments acquisition card (PCI-MIO-16XE-50) digitized and stored the PMT signal on a personal computer using a custom-written Labview program.

For diffusion measurements, a membrane was fastened using parafilm between two parts of a temperature-controlled aluminum chamber. Each compartment was filled with a buffer solution (0.01 M sodium phosphate buffer pH 7.5, volume 1.35 mL). The surface area of membrane exposed to the solution was 0.283 cm^2. The chamber was placed under the custom-built microscope and sealed from above to prevent evaporation. Temperature of the chamber was held constant by circulating water from a thermal bath through an inner space in the walls. Fluorescent polymer was injected to the *cis* side of the membrane (polymer concentration 7−15 μg/mL), and the time trace of fluorescence on the *trans* side was recorded. Bleaching was minimized by operating the LED in a pulsed mode with a short duty cycle. At the end of each experiment the solutions from the two sides were mixed to obtain the expected signal at equilibrium, i.e., at $t = \infty$. Homogeneity of the solutions was maintained by constant stirring with small magnetic bars.

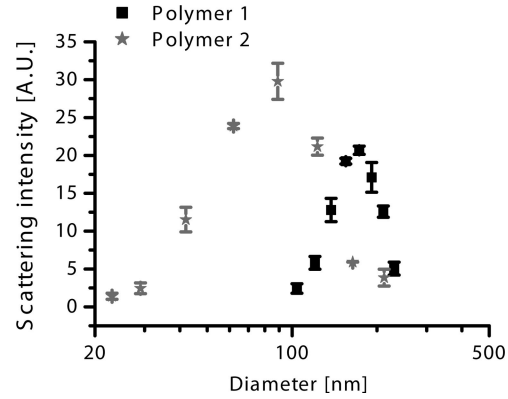

Figure 1. Hydrodynamic diameters of polymer 1 (black square) and polymer 2 (gray stars) as measured by dynamic light scattering.

PNIPAM transport behavior was compared to that of a widely used model polymer—low molecular weight dextran (Sigma-Aldrich 40 kDa, Stokes radius 4.5 nm).[51]

3. Results

Characterization of the Fluorescent Tagged Polymers. The hydrodynamic radii of polymers 1 and 2 were measured using dynamic light scattering (DLS). The CONTIN algorithm was used to analyze decay curves of the correlator.[52] Since the distribution determined by this algorithm may depend on initialization parameters, two separate measurements were performed on each sample, and two sets of initial parameters were used in their analysis. We obtained consistent results in each case. Summing the histograms of the separate measurements gave the size distributions shown in Figure 1. Gaussian fits yield $R_h = 85 \pm 40$ nm for polymer 1 and $R_h = 45 \pm 30$ nm for polymer 2.

The specific viscosity of polymer 1 was measured using a rotary viscosimeter at 20 °C and 10 mg/mL polymer solution. The average measured value is $\eta = 2.23 \pm 0.08$ cP. The average viscosity molecular weight ($\bar{M}_\eta$) can be calculated using the relation $[\eta] = 14.5 \times 10^{-2}\bar{M}_\eta^{0.5}$,[53] where $[\eta]$ is the specific viscosity in units of mL g^{-1}, with the result $\bar{M}_\eta = 714 \pm 3$ kDa. Using the average mass of a monomer on the chain (M), the viscosity average polymerization number $N_\eta \equiv \bar{M}_\eta/M = 5900 \pm 25$ is obtained, where the uncertainty reflects standard deviation over the mean rather than polydispersity. Since pNIPAM is a very flexible polymer, N_η can be used in order to estimate the Kuhn length (b). The relation $R_h = 0.64bN^{0.6}$ yields $b = 0.68 \pm 0.26$ nm; the contour length may be estimated as $bN = 4.0$ μm. The value of the Kuhn length is consistent with an independent measurement of the persistence length $L_p = {}^1/_2 b = 0.1-0.5$ nm using AFM and a wormlike chain model of pNIPAM.[54] Thus, the present DLS and viscosity results are consistent with other measures of pNIPAM flexibility.

Membrane Transport Experiment. The diffusion process of polymer 1 was measured using the classical setup of monitoring the *trans* side accumulation of solutes, with two homogenized solutions that are separated by a membrane and a higher solute concentration initially at the *cis* side.[6] The

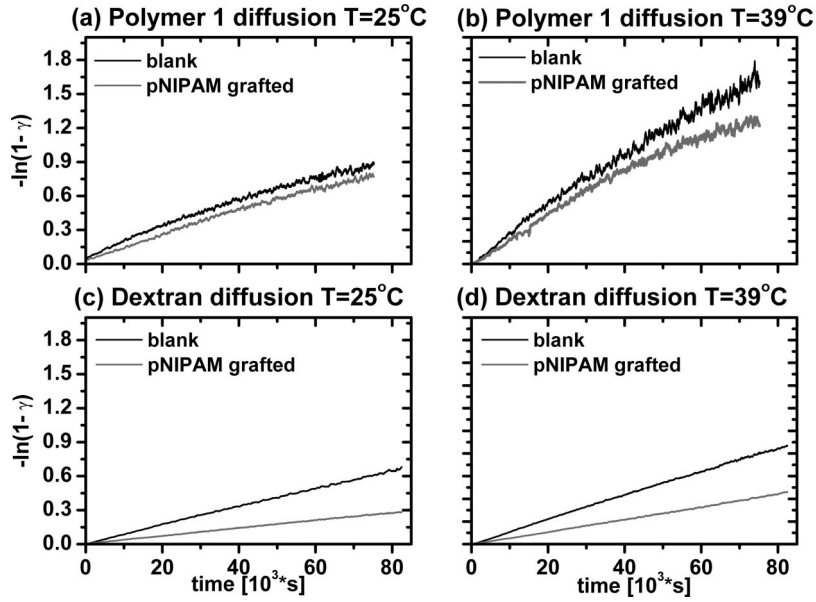

Figure 2. Time traces of fluorescent solute accumulation on the *trans* side of the membrane. *Y*-axis: $-\ln(1-\gamma)$, where γ is concentration normalized to equilibrium value; *X*-axis: time.Black lines = blank membrane; gray lines = chemically grafted membranes. (a, b) Fluorescent pNIPAM at 25 and 39 °C, respectively. (c, d) Fluorescent dextran at 25 and 39 °C, respectively.

fluorescence signal was used to quantify the solute concentration in the *trans* compartment. A calibration curve for pNIPAM appears in the Supporting Information (Figure S1b).

For the setup described above, a simple mathematical derivation for an ordinary intrapore diffusion process shows that the *trans* side accumulation should follow

$$C_{\text{trans}}(t) = C_{\text{f}}\left(1 - \exp\left(-\frac{2HDn}{LV}t\right)\right) \quad (1)$$

where V is the volume of one of the chamber compartments, L the width of the membrane, D the bulk diffusion constant, and n the number of available pores. $C(t)_{\text{trans}}$ is the time-dependent *trans* side concentration and C_{f} the expected final equilibrium concentration. The PMT counts is related to the concentration as $C \propto (\text{PMT}_{\text{counts}} - \text{PMT}_{\text{dark}})$, yielding

$$-\ln(1-\gamma) = \frac{2HDn}{LV}t \quad (2)$$

where $\gamma \equiv [\text{PMT}_{\text{counts}}(t) - \text{PMT}_{\text{dark}}]/[\text{PMT}_{\text{counts}}(t=\infty) - \text{PMT}_{\text{dark}}]$, $\text{PMT}_{\text{counts}}(t)$ are the counts of the PMT at time t, and PMT_{dark} is the average dark count of the PMT measured prior to the experiment.

Figures 2a,b show representative time traces of $-\ln(1-\gamma)$ for polymer 1, above and below the transition temperature. In all experiments the initial *cis* side concentration (7−15 μg/mL) was much below the overlap concentration (∼130 μg/mL). Two striking features are seen. First, the fluorescent pNIPAM diffused through the membrane even though $R_{\text{h}} > R_{\text{p}}$. This is a novel demonstration of fast diffusion inside cylindrical pores. Second, we observed a stretched exponential accumulation rate of the form $C_{\text{trans}} = C_f(1 - \exp(-At^{\beta}))$. A fit to the data determined $\beta = 0.77 \pm 0.04$ at $T = 25$ °C and 0.82 ± 0.04 at $T = 39$ °C (standard deviation from four experiments). The values of A were $(1.6 \pm 1.0) \times 10^{-4}$ s$^{-\beta}$ and $(1.2 \pm 0.5) \times 10^{-4}$ s$^{-\beta}$ at the low and high temperatures, respectively. Thus, the diffusion did not follow the expected behavior according to eq 2.

Figures 2c,d show representative time traces of $-\ln(1-\gamma)$ for dextran of relatively small hydrodynamic radius. In contrast to pNIPAM, dextran accumulation followed the expected linear form, with a hindrance diffusion factor $H = 0.86 \pm 0.04$, similar to previous reports.[4,55] The ratio between high and low temperatures, $D_{\text{p}}(39\ ^\circ\text{C})/D_{\text{p}}(25\ ^\circ\text{C}) = 1.4$, was entirely consistent with the expected ratio due to the change in solvent viscosity $(T_1\eta(T_2)/T_2\eta(T_1) = 1.4)$. Note that the level of accumulation of dextran was comparable to or even smaller than that of the much larger pNIPAM.

In principle, a stretched exponential accumulation could be obtained if one of the parameters determining the slope in eq 2 takes on a time dependence. Since the solution volumes were constant, the only two parameters that could change during the course of experiment are the hindrance diffusion factor (H) and the number of available pores (n). The former might change due to some sieving effect or due to concentration changes above the overlap concentration, while the latter might be related to plugging of the pores by adsorbed pNIPAM. Full details appear in the Supporting Information (Figures S2 and S3). Briefly, the experiment was performed below the polymer overlap concentration, size sieving was rejected on the basis of light scattering measurements of the *cis* and *trans* fractions separately, and pore plugging was ruled out by following fluorescent dextran together with an undetected pNIPAM.

We propose that the stretched exponential accumulation of polymer 1 is a result of the single chain intrapore diffusion mechanism. In particular, it may relate to the requirement for the polymer to deform in order to enter the pore. To test this hypothesis, we measured diffusion through membranes with progressively larger pores. Figure 3 shows polymer 1 accumulation for pores of diameter 200 nm ($R_{\text{h}}/R_{\text{p}} = 0.8$, i.e., of comparable size). As can be seen, the stretched exponential behavior is retained. The fit of $-\ln(1-\gamma)$ to a power law At^{β} gave the values $A = (2.4 \pm 1.2) \times 10^{-4}$ s$^{-\beta}$ and $\beta = 0.80 \pm 0.06$ (average and standard deviation of three experiments). Comparing the fitting values to the corresponding values of the smaller pores case, it can be seen that translocation rate was faster but that the anomalous characteristic of the diffusion was preserved.

For still larger pores of 1 μm ($R_{\text{h}}/R_{\text{p}} \ll 1$), the stretched exponential behavior approached a simple exponential. A typical example is shown as well in Figure 3. A fit of $-\ln(1-\gamma)$ to the power law form At^{β} yielded $\beta = 0.90 \pm 0.02$ and $A = (3 \pm 0.06) \times 10^{-5}$ s$^{-\beta}$ (three experiments). Interestingly, if we force a fit of $-\ln(1-\gamma)$ to linear form, we find $2HDn/LV = (9.4 \pm 2.2) \times 10^{-6}$ s^{-1}. This value is still ∼5 faster than what

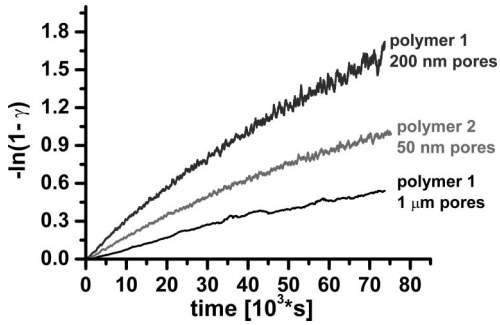

Figure 3. *Trans* side accumulation of polymer 1 at room temperature through polycarbonate membranes with 200 nm pores (dark gray) and 1000 nm (black). Gray: *trans* side accumulation of polymer 2 (cross-linked) at room temperature through polycarbonate membrane with 50 nm pores. Note that the area density of pores differs among the three membranes (Table 1). The normalized transport per pore is fastest for the 1000 nm and slowest for the 50 nm pores, as expected.

could have been expected based on the calculated value of $2Dn/LV$ (1.86×10^{-6} s^{-1}). Therefore, we note that the relative acceleration of diffusion with respect to the predicted rate through noninteracting pores decreased in comparison to the small pore case.

The diffusion mechanism of pNIPAM in narrow pores may also be studied by changing the structure of the polymer using the cross-linked polymer 2. Its *trans* side accumulation was measured at room temperature with 50 nm pore membranes. A typical example is shown in Figure 3. As can be seen, polymer 2 accumulation did not follow an exponential form but rather the stretched exponential form. A fit of the data to the equation gave $A = (1.6 \pm 0.15) \times 10^{-4}$ s$^{-\beta}$ and $\beta = 0.77 \pm 0.02$ (average and standard deviation of three experiments). These values are similar to those obtained for polymer 1 within experimental error. Thus, although their hydrodynamic radii were different, and although polymer 2 is at least 1% cross-linked, the diffusion rate was the same. This suggests that the translocation mechanism of the polymers inside the pores is also common in both cases and depends on some common parameter that is distinct from the hydrodynamic radius and the reduced entropy of the polymer inside the pore.

Adsorption of pNIPAM to Blank Polycarbonate Membrane. As discussed above, interactions with surfaces may induce a conformational phase transition of polymer chains. Such interactions can compensate for the entropy loss in confined geometries and even result in preferential residence of large polymers in nanopores. We proposed that such interactions are also the common factor responsible for pNIPAM intrapore diffusion characteristics by contributing to the initial stage of polymer translocation—the entrance into the pore.

In order to detect the polymer−pore interactions and to quantify their spatial distribution, we have used an adsorption assay based on fluorescence imaging. After incubation of a membrane in a solution of fluorescent tagged pNIPAM and extensive washing, the fluorescent and transmitted images of the surface were recorded using a confocal microscope. The fluorescence image appears granular, as can be seen in Figure 4a, indicating that the adsorption pattern is not uniform. In contrast, the adsorption pattern of the control polymer, the 40 kDa fluorescent dextran, is much less granular, as can be seen in Figure 4c.

Since the membrane surface is divided between the pores and the solid material, its transmission image is also inhomogeneous (Figures 4b,d). The relation between the nonuniformity in the adsorption pattern and the inhomogeneity of the membrane surface can be quantified using Pearson's correlation coefficient (P) defined by the relation $P = [\sum\sum(T_{mn} - \bar{T})(F_{mn} - \bar{F})]/[(\sum\sum(T_{mn} - \bar{T})^2)(\sum\sum(F_{mn} - \bar{F})^2)]^{1/2}$. Here T_{mn} and F_{mn} are the $\{m, n\}$ elements of the transmitted and fluorescence images, respectively, and $\bar{T}$ and $\bar{F}$ their average intensity. The value of P is limited by -1 for complete anticorrelation of intensity scale and by 1 for complete correlation. An absolute value of P close to zero indicates that the two figures are not correlated.

The calculated Pearson's coefficient for polymer 1 from five fields of view is $P = -0.18 \pm 0.05$, and the corresponding value for dextran is $P = -0.08 \pm 0.02$. The negative sign represents the inverse intensity between the pores in the transmission images (dark spots) and in the fluorescence images (bright spots). A Student t test with null hypothesis of identical correlation between the pNIPAM and dextran cases gave a probability smaller than 0.004. Thus, the measured Pearson's coefficient indicates significantly greater adsorption for pNIPAM in the holes than for dextran.

A further indication of pNIPAM adsorption inside the pores was obtained using a depth scan along the longitudinal dimension of the membrane. Fluorescent polymer is seen to traverse the membrane. An example is shown in Figures 4e,f. The z-axis sectioning of the confocal microscope is ~ 1 μm under the conditions employed.

Interestingly, for dextran with $R_h/R_p \leq 1$, the documented literature value of H in polycarbonate membranes was larger than predicted for solely hard wall interactions with the pore surface.[4] This was interpreted as evidence for attractive interactions with the pore walls. Assuming a van der Waals form of interactions, the functional dependence of H was fully described.[56] This indicates that pNIPAM interacts more strongly than dextran with the polycarbonate pores.

Transport in Grafted pNIPAM Membranes. The adsorption assay indicates that polymer 1 adsorbs partially on the pore walls. As discussed above, a slow exchange of adsorbed and soluble polymer may take place even when the adsorbed phase resists desorption into pure solvent. Moreover, the adsorbed chains constitute a modified pore surface with which pNIPAM from the *cis* side solution should interact, and these interactions should determine the intrapore diffusion. If this logic is correct, then the chemistry of the polycarbonate pore surfaces could be changed by a chemistry of isopropylacrylamide without changing the accumulation behavior of mobile pNIPAM. In order to test this, we have grafted a pNIPAM layer to the membranes by a "polymerization from" chemistry[57] as explained in the Experimental Section. Successful grafting of polymer on the membrane surface was detected using X-ray photoelectron spectroscopy (XPS). The analysis is presented in the Supporting Information (Section S3 and Figure S4).

Grafting of pNIPAM within the pores was resolved using a simple water flow assay and Poiseuille's law[57] to determine the effective pore diameter. We detected a narrowing from $\sim$47 nm, close to the nominal value of 50 nm, to $\sim$42 nm (Figure 5). No phase transition for the grafted polymer was observed over the temperature range 26−40 °C. Indeed, it is known that the transition might be suppressed for low molecular weight, grafted pNIPAM,[58−62] implying that the exposed, grafted polymer is in a hydrophilic state on the membrane.

We then compared dextran and pNIPAM transport through the pNIPAM-grafted membranes with the measurements through untreated membranes. The rate of dextran passage was clearly reduced by the grafting. Typical examples are shown in Figures 2c,d. The variance of the passage rate also increased with grafting, which suggests slight differences from sample to sample. At 25 °C we measured an average $H = 0.45 \pm 0.13$ (eight experiments), and for 39 °C $H = 0.46 \pm 0.06$ (seven experiments); the similarity is consistent with the water flow measurement and the lack of a phase transition in the grafted

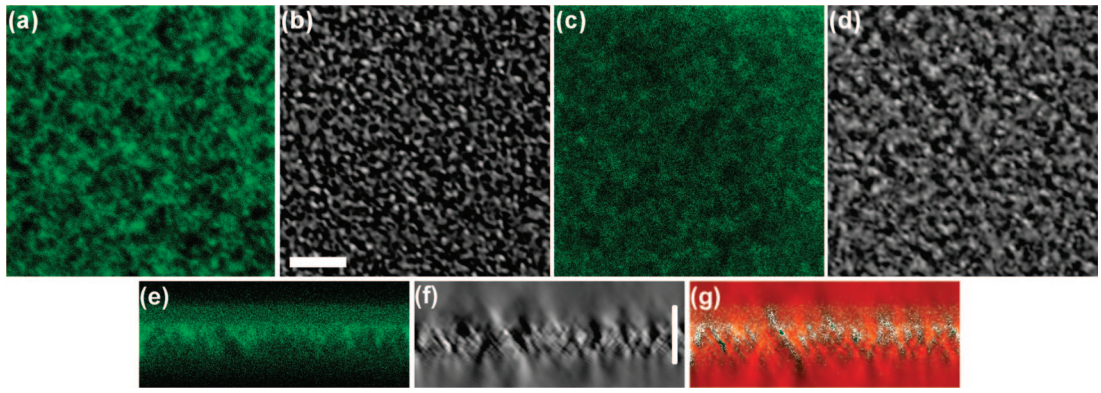

Figure 4. Adsorption assays for quantification of the spatial dependence of interaction between polymers and the polycarbonate membranes using confocal microscopy. Images were recorded after 2 days of incubation with the polymers. (a) Fluorescence image of polymer 1 adsorption. (b) Transmission image of the same field of view (FOV). (c) and (d) are the same as (a) and (b) for dextran adsorption. (e) Fluorescent channel depth scan along the membrane longitudinal direction. (f) Transmission channel depth scan for the same FOV. (g) Colocalization figure of (e) and (f) according to the procedure described in the text. (a)−(d) have the same scale (shown in (b)). (e)−(g) have same scale bar (shown in (f)). In both cases the scale bar is 5 μm.

polymer. Measurements of the *trans* side accumulation of polymer 1 through pNIPAM-grafted membranes showed the same stretched exponential behavior and a similar rate as in the ungrafted case (Figures 2a,b). For the grafted membranes we measured $\beta = 0.78 \pm 0.05$; $A = (1.0 \pm 0.6) \times 10^{-4}$ s$^{-\beta}$ at low temperature (seven experiments), and $\beta = 0.91 \pm 0.07$; $A = (0.4 \pm 0.5) \times 10^{-4}$ s$^{-\beta}$ at high temperature (four experiments). Thus, we were able to change the chemistry of the pore surfaces, hindering the passage of dextran but hardly affecting that of pNIPAM. These results confirm the prediction that pNIPAM diffusion through the small pores is chemically specific, depending on interactions with either the adsorbed or the grafted immobile pNIPAM layer.

4. Discussion

The Diffusion Mechanism. In the absence of surface interactions, the loss of conformational entropy would have been too large to allow the pNIPAM polymers discussed here to enter or pass through 50 nm narrow pores. Polymers may pass through pores much smaller than their hydrodynamic size when induced by an external field. For example, flow-driven translocation in ultrafiltration,[63] or electric field-driven translocation for charged polymers,[8] can result in stretching and passage through a pore in an extended conformation. The applied extension balances the entropic contribution to the free energy. After the polymer enters a pore the external force continues to drag it through. Interestingly, excluded volume interactions or entropic forces may cause polymer unfolding even if the external forces are switched off.[64] In the present case, however, no external force was applied to drive the polymer into the pore. We nonetheless observed passage through the pores with a substantial rate compared to the much smaller dextran. Thus, two aspects of the translocation process should be considered: entrance into the pore and translocation inside the channel.

The adsorption assay showed that pNIPAM is attracted to the pore walls. This explains the initial stage of polymer entry. Even if the solution concentration is below overlap, the local accumulation of pNIPAM will be higher. The mobile polymer could exchange with the adsorbed one by the piecewise mechanism described above.[29] This would permit a turnover within the pore and translocation even in the presence of adsorption. However, we observed similar kinetics with the grafted pores where the stationary phase was permanently bound. In that case, transient intrapolymeric interaction with the grafted phase could still explain the initial stage of entrance, but an exchange mechanism between free polymer and surface bounded polymer is not a feasible explanation for the intrapore diffusion mechanism. In addition, since the contour length of polymer 1 is less than the thickness of the membrane, the driving force for translocation is not supplied by adsorption of the chain to the outer surface of the membrane.[65] Hence, we attribute the initial stage of entrance into the pore and the corresponding stretching to interaction between the stationary and free polymer phase near the pore entrance. In addition, since no external force was applied, we attribute the intrapore diffusion mechanism to attractive transient hydrophobic and hydrogen bonds between the mobile and stationary pNIPAM phases. We consider these to be the most likely driving source for translocation at the microscopic level.

In the past, the ordinary theory of solute diffusion through narrow pores was applied for macromolecules if H_D and Θ were calculated from polymer physics considerations.[6] Even including attractive interactions between the polymer and the pore surfaces the theory could still be applied, as was shown for dextran with R_h equal to R_p.[4] The measured value of H was larger than the predicted one for hard wall interactions, yet the intrapore diffusion was not anomalous.[56] In our case, a stretched exponential accumulation was measured. This may reflect a different regime of surface interaction relevant to dextran and pNIPAM. Passage of dextran is normally treated without consideration of adsorption. pNIPAM translocation would differ qualitatively if its surface interaction lies in a regime of strong or critical adsorption.

We recall that reptation is a characteristic diffusion mechanism of polymers next to a strongly adsorbing planar surface. Here, we have shown that the partially cross-linked polymer 2 passes the pores with a similar rate to polymer 1 and follows the same anomalous scaling in accumulation. Diffusion by pure reptation is not possible for a cross-linked polymer, so this suggests that reptation along the pore surface did not play an important role in our measurements. Additionally, serpentine diffusion on an adsorbing surface should display a power law molecular weight dependence. In that case, the passage of the polydisperse polymer 1 should have shown a strong sieving effect. Instead, relatively longer and shorter chains in the polydisperse sample diffused with the same kinetics. The experimental evidence thus weighs against the suggestion of diffusion in a regime of strong surface adsorption.

We therefore suggest that the pNIPAM in pNIPAM-coated pores, exhibiting pNIPAM−pNIPAM interactions, lies in the critical regime of adsorption. In this regime, the number of monomers for a Gaussian chain in a layer of one monomer width

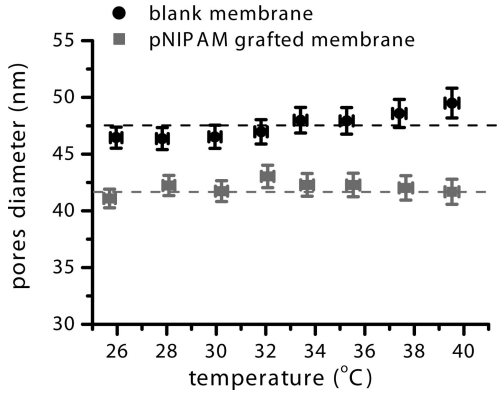

Figure 5. Effective membrane pore diameters as measured by water permeability using Poiseuille's law, before and after grafting. Dashed lines are guides to the eye.

(*a*) is $Q \simeq (a/R_p)[1 + (2R_p/3)s]$, where s is the inverse adsorption correlation length.[16] For example, at the critical point ($s = 0$) we estimate that $Q \simeq 100$ monomers are available to form surface bonds. This suggests that a significant number of monomers will be in contact with the surface, consistent with a geometry of lampbrush loops.[47,48] In order for the center of mass of the polymer to perform one diffusion step, a coordinated or a continuous rupture of these many surface bonds and the formation of new bonds should occur. As a result, the polymer would be subject to multiple trapping events. This criterion should, on general grounds, introduce multiple characteristic times into the diffusion process.[66,67] In the framework of the continuous time random walk, the waiting time distribution between successive steps is defined as the fundamental parameter of the diffusion mechanism. Anomalous diffusion arises naturally if the tail of this distribution becomes long, as would be expected for multiple trapping.[68] The number of potential surface bonds Q depends inversely on R_p. In wide pores the much smaller number of surface bonds may considerably narrow the characteristic trapping time. In that case the transport should approach an ordinary diffusion with the mean value of the probability distribution between steps being the maximal trapping time. Indeed, pNIPAM diffusion through wide pores approached an ordinary diffusion.

5. Conclusion

We have shown that a large molecular weight pNIPAM diffuses through pores that are narrower than its hydrodynamic diameter. Transient hydrophobic and hydrogen bond interactions between the mobile polymer and the pore walls appear to play an important role in the anomalous kinetics. Interpolymer hydrogen bonding provides a mechanism for attractive surface interaction that compensates for a loss of configuration entropy in the mobile polymer. This may accelerate the rate of passage while introducing a subdiffusive time scaling, i.e., anomalous diffusion. The noninteracting dextran did not show these anomalous features and passed the pores more slowly than the pNIPAM in spite of its much smaller size. Further theoretical and experimental studies are needed in order to derive the anomalous diffusion constant and scaling exponent from first principles of polymer physics.

Acknowledgment. The authors thank Ellen Wachtel for assistance with light scattering measurements, and Yitzhak Rabin for illuminating discussions. This work was supported in part by a grant from the Israel Science Foundation and by the Gerhardt M. J. Schmidt Minerva Center for Supramolecular Architecture. This research is made possible in part by the historic generosity of the Harold Perlman family.

Supporting Information Available: Setup sketch, setup calibration curve, comparison of dextran accumulation in the presence and absence of high molecular weight pNIPAM, comparison of pNIPAM size distribution of the *cis* and *trans* sides, and XPS analysis of the surfaces. This material is available free of charge via the Internet at http://pubs.acs.org.

References and Notes

(1) Teraoka, I. *Prog. Polym. Sci.* **1996**, *21*, 89–149.
(2) Cannell, D. S.; Rondelez, F. *Macromolecules* **1980**, *13*, 1599–1602.
(3) Deen, W. M.; Bohrer, M. P.; Epstein, N. B. *AIChE J.* **1981**, *27*, 952–959.
(4) Bohrer, M. P.; Patterson, G. D.; Carroll, P. J. *Macromolecules* **1984**, *17*, 1170–1173.
(5) Guillot, G.; Leger, L.; Rondelez, F. *Macromolecules* **1985**, *18*, 2531–2537.
(6) Deen, W. M. *AIChE J.* **1987**, *33*, 1409–1425.
(7) Noordman, T. R.; Wesselingh, J. A. *J. Membr. Sci.* **2002**, *210*, 227–243.
(8) Tegenfeldt, J. O.; et al. *Proc. Natl. Acad. Sci. U.S.A.* **2004**, *101*, 10979–10983.
(9) Oukhaled, G.; Mathé, J.; Biance, A. L.; Bacri, L.; Betton, J. M.; Lairez, D.; Pelta, J.; Auvray, L. *Phys. Rev. Lett.* **2007**, *98*, 158101.
(10) Daoud, M.; de Gennes, P. G. *J. Phys. II* **1977**, *38*, 85–93.
(11) Harden, J. L.; Doi, M. *J. Phys. Chem.* **1992**, *96*, 4046–4052.
(12) Guillot, G. *Macromolecules* **1987**, *20*, 2600–2606.
(13) Guillot, G. *Macromolecules* **1987**, *20*, 2606–2614.
(14) Song, Q.; Zhang, G.; Wu, C. *Macromolecules* **2007**, *40*, 8061–8065.
(15) Lin, N. P.; Deen, W. M. *Macromolecules* **1990**, *23*, 2947–2955.
(16) Gorbunov, A. A.; Skvortsov, A. M. *Adv. Colloid Interface Sci.* **1995**, *62*, 31–108.
(17) Cifra, P.; Bleha, T. *Polymer* **2000**, *41*, 1003–1009.
(18) Wang, Y.; Howard, D.; Yingchuan, G. *Polymer* **2004**, *45*, 313–320.
(19) Grull, H.; Shaulitch, R.; Yerushalmi-Rozen, R. *Macromolecules* **2001**, *34*, 8315–8320.
(20) Berek, D. *Prog. Polym. Sci.* **2000**, *25*, 873–908.
(21) Eisenriegler, E. *Polymers near Surfaces*; World Scientific: Singapore, 1993.
(22) Sukhishvili, S. A.; Chen, Y.; Müller, J. D.; Gratton, E.; Schweizer, K. S.; Granick, S. *Nature (London)* **2000**, *406*, 146.
(23) Kumaki, J.; Kawauchi, T.; Yashima, E. *Macromolecules* **2006**, *39*, 1209–1215.
(24) Milchev, A.; Binder, K. *Macromolecules* **1996**, *29*, 343–354.
(25) Wolterink, J. K.; Barkema, G. T.; Stuart, M. A. C. *Macromolecules* **2005**, *38*, 2009–2014.
(26) Desai, T. G.; Keblinski, P.; Kumar, S. K. *J. Chem. Phys.* **2008**, *128*, 044903.
(27) Mukherji, D.; Bartels, G.; Muser, M. H. *Phys. Rev. Lett.* **2008**, *100*, 068301.
(28) Frantz, P.; Granick, S. *Phys. Rev. Lett.* **1991**, *66*, 899–902.
(29) Pefferkorn, E.; Haouam, A.; Varoqui, R. *Macromolecules* **1989**, *22*, 2677–2682.
(30) Johnson, H. E.; Granick, S. *Science* **1992**, *255*, 966–968.
(31) Milchev, A.; Paul, W.; Binder, K. *Macromol. Theory Simul.* **1994**, *3*, 305–323.
(32) Milchev, A.; Binder, K. *J. Comput.-Aided Mater. Des.* **1995**, *2*, 167–181.
(33) Schönhals, A.; Goering, H.; Schick, C. *J. Non-Cryst. Solids* **2002**, *305*, 140–149.
(34) Berezhkovskii, A. M.; Bezrukov, S. M. *Chem. Phys.* **2005**, *319*, 342–349.
(35) Denning, D. P.; Patel, S. S.; Uversky, V.; Fink, A. L.; Rexach, M. *Proc. Natl. Acad. Sci. U.S.A.* **2003**, *100*, 2450–2455.
(36) Rout, M. P.; Aitchison, J. D.; Magnasco, M. O.; Chait, B. T. *Trends Cell Biol.* **2003**, *13*, 622–628.
(37) Zilman, A.; Talia, S. D.; Chait, B. T.; Rout, M. P.; Magnasco, M. O. *PLoS Comput. Biol.* **2007**, *3*, 1281–1290.
(38) Frey, S.; Görlich, D. *Cell* **2007**, *130*, 512–523.
(39) Lim, R. Y.; Köser, J.; Huang, N.-p.; Schwarz-Herion, K.; Aebi, U. *J. Struct. Biol* **2007**, *159*, 277–289.
(40) Kopito, R. B.; Elbaum, M. *Proc. Natl. Acad. Sci. U.S.A.* **2007**, *104*, 12743–12748.
(41) Schild, H. G. *Prog. Polym. Sci.* **1992**, *17*, 163–249.
(42) Katsumoto, Y.; Tanaka, T.; Ozaki, Y. *Macromol. Symp.* **2004**, *205*, 209–223.
(43) Kimhi, O.; Bianco-Peled, H. *Langmuir* **2002**, *18*, 8587–8592.
(44) Wu, C.; Wang, X. *Phys. Rev. Lett.* **1998**, *80*, 4092–4094.
(45) Xu, J.; Zhu, Z.; Luo, S.; Wu, C.; Liu, S. *Phys. Rev. Lett.* **2006**, *96*, 027802.
(46) Ye, X.; Lu, Y.; Shen, L.; Ding, Y.; Liu, S.; Zhang, G.; Wu, C. *Macromolecules* **2007**, *40*, 4750–4752.

(47) Zhu, P. W.; Napper, D. H. *Phys. Rev. E* **1998**, *57*, 3101–3106.
(48) Zhu, P. W.; Napper, D. H. *Macromol. Chem. Phys.* **1999**, *200*, 698–705.
(49) Ferruti, P.; Fere, A.; Bettelli, A. *Polymer* **1972**, *13*, 462–464.
(50) http://rsb.info.nih.gov/ij/.
(51) http://www.sigmaaldrich.com/sigma/product%20information%20sheet/fd40spis.pdf.
(52) Provencher, S. W. *Macromol. Chem. Phys.* **1979**, *180*, 201–209.
(53) Fujishige, S. *Polym. J.* **1987**, *19*, 297–300.
(54) Haupt, B. J.; Senden, T. J.; Sevick, E. M. *Langmuir* **2002**, *18*, 2174–2182.
(55) Lebrun, L.; Junter, G.-A. *J. Membr. Sci.* **1994**, *88*, 253–1.
(56) Shao, J.; Baltus, R. E. *AIChE J.* **2000**, *46*, 1149–1156.
(57) Xie, R.; Chu, L.-Y.; Chen, W.-M.; Xiao, W.; Wang, H.-D.; Qu, J.-B. *J. Membr. Sci.* **2005**, *258*, 157–166.
(58) Yim, H.; Kent, M. S.; Huber, D. L.; Satija, S.; Majewski, J.; Smith, G. S. *Macromolecules* **2003**, *36*, 5244–5251.
(59) Yim, H.; Kent, M. S.; Mendez, S.; Lopez, G. P.; Satija, S.; Seo, Y. *Macromolecules* **2006**, *39*, 3420–3426.
(60) Yim, H.; Kent, M. S.; Mendez, S.; Balamurugan, S. S.; Balamurugan, S.; Lopez, G. P.; Satija, S. *Macromolecules* **2004**, *37*, 1994–1997.
(61) Plunkett, K. N.; Zhu, X.; Moore, J. S.; Leckband, D. E. *Langmuir* **2006**, *22*, 4259–4266.
(62) Zhu, X.; Yan, C.; Winnik, F. M.; Leckband, D. *Langmuir* **2007**, *23*, 162–169.
(63) Jin, F.; Wu, C. *Phys. Rev. Lett.* **2006**, *96*, 237801.
(64) Levy, S. L.; Mannion, J. T.; Cheng, J.; Reccius, C. H.; Craighead, H. G. *Nano Lett.* **2008**, *8*, 3839–3844.
(65) Milchev, A.; Binder, K.; Bhattacharya, A. *J. Chem. Phys.* **2004**, *121*, 6042–6051.
(66) Palmer, R. G.; Stein, D. L.; Abrahams, E.; Anderson, P. W. *Phys. Rev. Lett.* **1984**, *53*, 958–961.
(67) Klafter, J.; Shlesinger, M. F. *Proc. Natl. Acad. Sci. U.S.A.* **1986**, *83*, 848–851.
(68) Metzler, R.; Klafter, J. *Phys. Rep.* **2000**, *339*, 1–77.

MA801248A